JPE 14-1-12

http://dx.doi.org/10.6113/JPE.2014.14.1.115
ISSN(Print): 1598-2092 / ISSN(Online): 2093-4718

Implementation of Space Vector Two-Arm Modulation for Independent Motor Control Drive Fed by a Five-Leg Inverter

Md Hairul Nizam Talib[†], Zulkifilie Ibrahim[*],
Nasrudin Abd. Rahim[**], and Ahmad Shukri Abu Hasim[***]

[†*]Faculty of Electrical Engineering, Universiti Teknikal Malaysia Melaka, Melaka, Malaysia
[**]UMPEDAC, Universiti Malaya, Kuala Lumpur, Malaysia
[***]Faculty of Engineering, Universiti Pertahanan Nasional Malaysia, Kuala Lumpur, Malaysia

Abstract

This paper presents the implementation of two-arm modulation (TAM) technique for the independent control of a two-induction motor drive fed by a five-leg inverter (FLI). A carrier-based space vector pulse width modulation technique for TAM is proposed to generate switching signals for FLI. Two independent three-phase space vector modulators are utilized to control two motors. The motor drive system applies two separate indirect field-oriented control methods. The stationary voltage outputs from the vector control are synthesized in the three-phase space vector modulator to generate switching signals for FLI. The performance of the independent control of the motors and the voltage utilization factor are likewise analyzed. Simulation and experimental results verify the effectiveness of the proposed method for the independent control of the two-motor drive system. The proposed technique is successfully validated by dSPACE DS1103 experimental work.

Keywords: Five-Leg Inverter, Induction Motor Drive, Two-Arm Modulation, Space Vector Pulse Width Modulation

I. INTRODUCTION

Two or more motors may be used or operated for different applications in industries. Some applications require different speeds and torque operations. Conventional one-motor control drive systems are commonly used for these applications. However, the independent control of two-motor drive systems by a single five-leg inverter (FLI) also fulfills the requirement. The system helps decrease the number of used power switch components to only one DC bus supply and one controller. In addition, the system occupies minimal space and is not complex. The proposed solution is significant mainly for industrial applications that require multiple drive systems, such as six-axis industrial robots, machine tools, and winding machines.

Manuscript received Jul. 23, 2013; revised Oct. 17, 2013
Recommended for publication by Associate Editor Lixiang Wei.
[†]Corresponding Author: hairulnizam@utem.edu.my
Tel: +60-65552233, Universiti Teknikal Malaysia Melaka
[*]Faculty of Electrical Engineering, Universiti Teknikal Malaysia Melaka, Malaysia
[**]UMPEDAC, Universiti Malaya, Malaysia
[***]Faculty of Engineering, Universiti Pertahanan Nasional Malaysia, Malaysia

The five-leg voltage source inverter configuration consists of five parallel legs of paired IGBTs parallel to the DC power supply or DC link capacitor. This configuration has 10 IGBTs compared with the six IGBTs in conventional three-leg inverter systems. In conventional drive systems, 12 IGBTs are required for two-motor operations. One leg is shared with one motor supply in the independent control of two-motor applications. Leg 3 or 5 is normally used as the common leg [1]–[12]. Thus, FLI saves one leg to control two-motor systems compared with conventional motor control methods.

Numerous pulse width modulation (PWM) techniques are employed in FLI topology. Among these methods are dual voltage modulation, modulation block method, inversion table method, and double zero sequence method (DZS) [2], [13]–]16]. DZS is the one of the best methods that enables the arbitrary distribution of the DC link voltage between two motors to maintain the operation in constant switching frequency mode. In addition, DZS is simple and easy to implement using standard DSP. This method can overcome the drawback of previous PWMs, such as the restriction of 50% of the DC bus voltage for one motor, asymmetrical

switching frequency, underutilization of the switching state, sideband harmonics, high-magnitude THD generation, and the complexity problem. DZS method can be implemented either by carrier-based technique or space vector pulse width modulation (SVPWM) technique [2], [17].

Two-arm modulation (TAM) is another popular method utilized for FLI modulation [7]–[11]. A similar connection structure is employed where one leg is shared for the motor connection. The advantages of this method are the independent control of the motors, easy implementation in DSP, and constant switching frequency. The method has similar advantages to DZS but employs different approaches to produce PWM modulation signals for FLI, especially for voltage distribution. Most studies have focused on sinusoidal pulse width modulation (SPWM) techniques [7]–[10], [17].

The workability of the space vector and the DC voltage utilization effect in FLI systems are analyzed in this study. SVPWM is a more appropriate modulation strategy than the SPWM technique for the conventional three-leg voltage source inverter system. SVPWM exhibits superior performance in reducing the harmonic of the output voltage, reduces switching losses, and increases output voltage [18–22]. SVPWM can achieve 15% higher output voltage than SPWM. Full utilization of the DC bus voltage is extremely important to achieve the maximum output torque under all operational conditions.

SVPWM for two-arm modulation was proposed by A. Hara [10] in 2011. A detailed design of SVPWM for FLI was presented, and experimental results for SPWM and SVPWM under no load operation were obtained and compared. SVPWM method was able to reduce gate signals unlike the carrier-based technique. Sampling time was separated into two parts: modulation and zero-voltage vector parts. Thus, the motor was controlled accordingly within the sampling time. However, the SVPWM gate signal was different from that of the conventional three-leg inverter SVPWM technique.

A carrier-based SVPWM technique with two-arm modulation based on two individual three-phase space vector modulators is proposed in the present study. Modulation signals are utilized to control FLI in the independent control of the two-motor system. The proposed technique is validated by dSPACE DS1103 experimental work.

II. FIVE-LEG INVERTER

A. Overall Block Diagram

The overall block diagram of the two-motor control system fed by FLI is shown in Fig. 1. The system generally applies two individual vector control methods to control two three-phase induction motors. The output signals of the voltage regulators of M1 and M2 are then combined in the five-leg modulation technique to generate signals to drive FLI. In the SVPWM method, dq to αβ transformation blocks

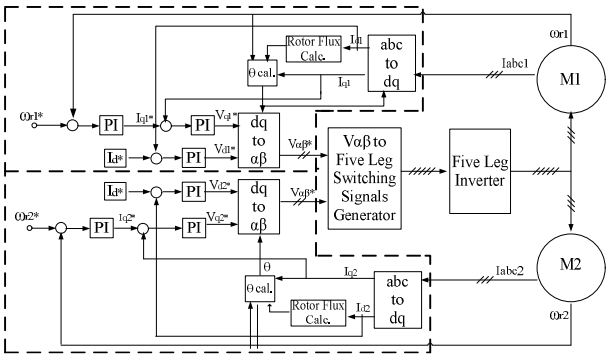

Fig. 1. Diagram of the two-induction motor drive vector control block.

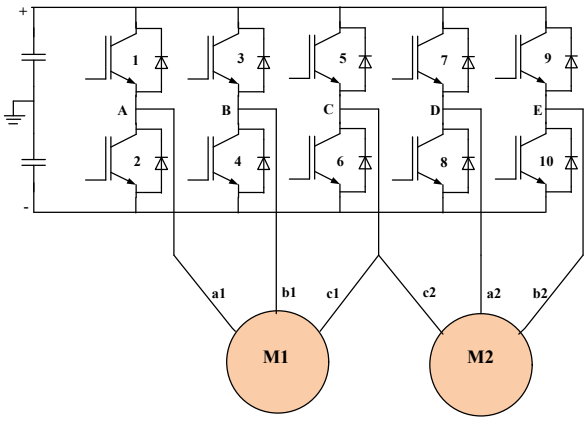

Fig. 2. Connection between the five-leg inverter and the motors [13].

are utilized as shown in Fig. 1. In the SPWM technique, dq to abc transformation blocks are employed. The output voltages of FLI control the operation of the motors.

B. FLI Configuration

A typical connection of the five-leg voltage source inverter to the two three-phase induction motors is shown in Fig. 2. Each leg consists of two switches, with a total number of ten switches. Inverter legs A and B are connected to M1, and legs D and E are connected to M2. In the FLI topology, one leg is utilized as the common leg. This common leg is shared by both motors. In this case, leg C is selected as the common leg. All the legs are connected to the three-phase supply termination of the motors denoted as a1, b1, c1 and a2, b2, c2 to represent M1 and M2 termination, respectively. The common leg experiences high current because of the sum of the phase current of the two motors and the harmonics content. However, in some specific applications, such as winders [1, 2], the two motors never operate simultaneously with full load current; this requirement can be tolerated.

C. SPWM for TAM

This method was proposed by [7] and is shown in the block diagram in Fig. 3. For this analysis, similar structures

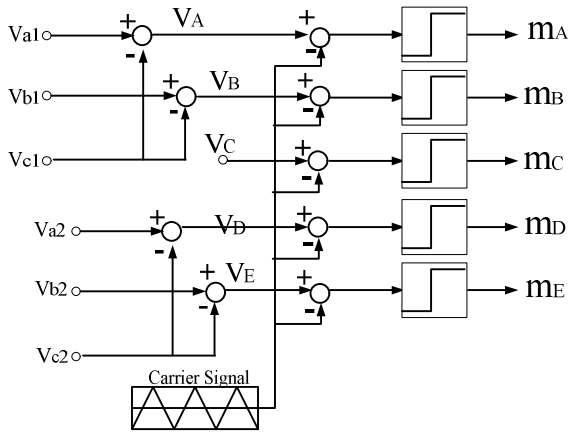

Fig. 3. Block diagram of SPWM for two-arm modulation.

of FLI and motor connections are used, where leg C is used as the common leg.

The phase a1 and phase b1 voltages of the fundamental sinusoidal reference signals are compared with the fundamental signal of the phase c1 voltage of the set 1 supply based on the block diagram of SPWM TAM. This process is also implemented for the set 2 fundamental voltage reference denoted as V_{a2}, V_{b2}, and V_{c2}. The output signal can be expressed as

$$\begin{aligned} V_A &= V_{a1}(t) - V_{c1}(t), \\ V_B &= V_{b1}(t) - V_{c1}(t), \\ V_D &= V_{a2}(t) - V_{c2}(t), \\ V_E &= V_{b2}(t) - V_{c2}(t). \end{aligned} \tag{1}$$

In TAM method, the common leg of phase C is connected to zero signal voltage, which can yield a 50% duty cycle of the switching signal [9]. Finally, the signal modulation output is compared with the carrier signals to produce five modulation signals denoted as m_A, m_B, m_C, m_D, and m_E. These modulation signals are applied to control the switching of FLI for the two-motor control operation.

D. Proposed SVPWM TAM Method

Fig. 4 shows the block diagram of the proposed carrier-based SVPWM TAM. This method utilizes the standard three-phase space vector modulator to generate modulation signals for FLI. Based on this principle, the first set of the fundamental voltages in the stationary frame is synthesized in the three-phase space vector modulator. The output of the first space vector modulator is three modulator signals denoted as δa1, δb1, and δc1. The second modulator signal sets are denoted as δa2, δb2, and δc2.

Based on the TAM principle, the modulator signal outputs of δa1 and δb1 are deducted with modulator output δc1 for the set 1 modulator. This process is repeated for set 2 as shown in Equation (2). Processes similar to those in the SPWM TAM methods discussed above are repeated to

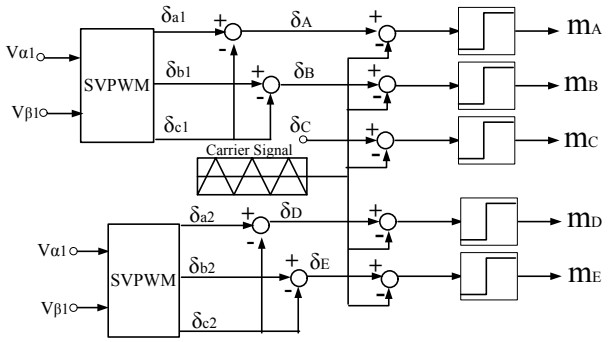

Fig. 4. Vαβ to the five-leg switching signal generator based on the block diagram of two-arm modulation.

TABLE I
INDUCTION MOTOR PARAMETERS

Motor Specifications	Value
Rated Voltage	380 V
Rated Frequency	50 Hz
Poles	4
Rated Speed	1430 rpm
Stator Resistance	3.45 Ω
Rotor Resistance	3.6141 Ω
Stator Inductance	0.3246 H
Rotor Inductance	0.3252 H
Magnetizing Inductance	0.3117 H
Inertia	0.02 kgm^2
Viscous Friction	0.001 Nm/(rad/s)

produce five modulation signals for the gate drives.

$$\begin{aligned} \delta_A &= \delta_{a1} - \delta_{c1} \\ \delta_B &= \delta_{b1} - \delta_{c1} \\ \delta_D &= \delta_{a2} - \delta_{c2} \\ \delta_E &= \delta_{b2} - \delta_{c2} \end{aligned} \tag{2}$$

III. SIMULATION SETUP AND RESULT

Simulations are performed for the two-motor controls for FLI through SPWM and SVPWM by TAM methods. A dedicated speed profile is applied to investigate the performance of the PWM methods with regard to motor performance. A similar simulation model of induction motor vector control drive is used to allow a fair comparison of the different PWM techniques. All the components are modeled in Simulink/Matlab. The first test is implemented by SPWM TAM method and the second test by SVPWM TAM method. The following are the details of the parameters and scheme

TABLE II
PI CONTROLLER PARAMETERS

PI Controller	Value
Speed Controller	Kp=0.135 Ki=0.4252
Flux Controller	Kp=4.65 Ki=8.94
Torque Controller	Kp=13.43 Ki=197.45

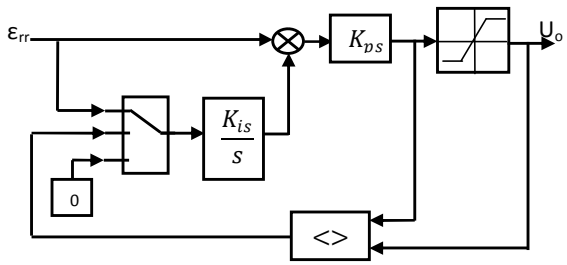

Fig. 5. AWPI condition.

employed in the simulation and experiment.

A. MOTOR PARAMETERS

Two similar three-phase induction motors are utilized in the simulation and experiments. The details of the motor parameters are shown in Table I.

B. PI Controller

Referring to the vector control block diagram in Fig. 1, three PI controllers are used for the speed, torque, and flux components controlled for each single motor control. A similar scheme and parameter value of the PI controllers are used in the first and second tests. The values are determined with the second-order general equations method. Damping ratio ς is set to 1, and natural frequency fn is set to 100, 10, and 1 Hz for the torque, flux, and speed control loops, respectively. Table II shows the PI controller parameters for the speed, torque, and flux components.

C. Anti-Wind-Up Scheme for Speed Control

An anti-wind-up scheme is applied at the speed control to improve overshoot and settling time. The scheme can avoid the over-value in the integrator that causes the windup phenomenon. This phenomenon results from the inconsistency between the real plant input and the controller output. To overcome the wind-up problem, the integral state is controlled separately depending on whether the PI controller output is saturated based on the anti-wind-up structure in 0. It is also applicable to any situation characterized by considerable step changes or where large external load disturbance saturates the PI controller.

D. Simulation Results

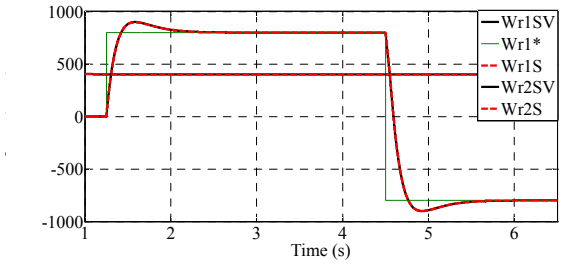

Fig. 6. Simulation results comparing the motor speed responses of M1 and M2 operation during standstill and at forward and reverse directions at 800 rpm speed operation by SPWM and SVPWM TAM methods.

According to the principle of the two-induction motor drive fed by FLI, the summed voltage requirement of both motors must be within the DC bus voltage supply. Thus, simulation is performed based on the step input speed reference for the forward and reverse operations by abiding by this principle to understand the speed behavior. The DC supply is set to 560 V, and the switching frequency is set to 6 kHz. Fig. 6 shows the speed response when the step speed reference is applied to motor M1 from zero speed to 800 rpm at 1.25 s for forward motor operation and suddenly changed to 800 rpm in the reverse direction at 4.5 s. The M2 motor operates at a fixed speed of 400 rpm. The last characters of the legend, namely, S, SV, and *, represent SPWM, SVPMW, and the reference. The results show that the motor tracks the command speed with almost zero speed error during steady state with similar settling time for all speed operations for SPWM and SVPWM TAM.

Figs. 7(a) and 7(b) show the torque current Iq for M1 and M2 using SPWM and SVPWM TAM. For motor M1, both torque currents reached a limited 10 A set at the speed controller during the step change demand. The response shows identical response time. The Iq2 current run at constant values does not affect the current change in Iq1. This result reveals the independence of the two motors, which are fully decoupled. Similar current performance for the M1 and M2 motors is recorded for SPWM and SVPWM, with a 0.25 Ap-p current ripple.

All the phase voltages are recorded to investigate the voltage output behavior of the techniques. Figs. 8(a) and 8(b) show the phase A voltage waveform for motor M1 using SPWM and SVPWM, respectively. Based on the waveform, nearly similar waveform patterns are produced with minor differences in the location of the spike voltage.

Fast Fourier transform (FFT) analysis is conducted to analyze the voltage waveforms. Twenty cycles of steady-state voltages are selected for the analysis starting at 3.5 s. To obtain a better view of the harmonics spectrum, the frequency is limited to 100 Hz, and the magnitude is limited to 10% of the fundamental components. Figs. 9(a) and 9(b) show the harmonics spectrum of phase A voltage using

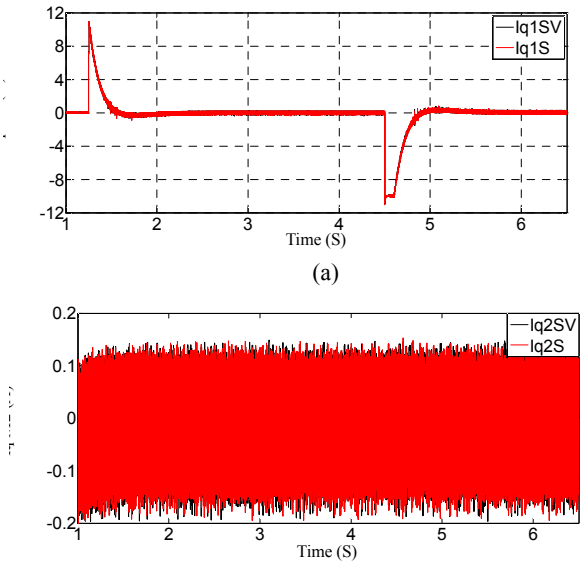

Fig. 7. Simulation results comparing torque current Iq of the demands using both techniques. (a) Torque current for M1 and (b) torque current for M2.

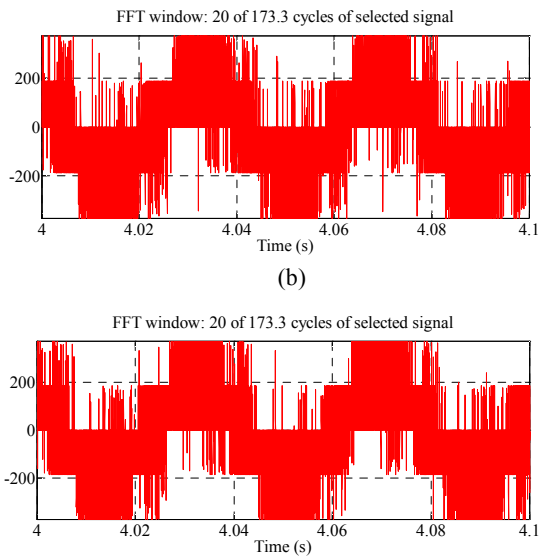

Fig. 8. Simulation results of Phase A voltage waveform for M1 using (a) SPWM technique and (b) SVPWM technique.

SPWM and SVPWM, respectively. The results show that almost similar fundamental rms voltages are recorded at 102.8 and 102.3 V for SPWM and SVPWM, respectively. Meanwhile, SVPWM produces less THD compared with SPWM, with a 0.76 difference. Both techniques produce a high third-order harmonic even with SVPWM because of the cancelation of the zero-voltage components for SVPWM.

Table III shows the FFT analysis for the phase voltages of M1 using SPWM and SVPWM. The FFT results show that the voltage output value produced by these two techniques is inconsistent. Slight differences exist because of the minor

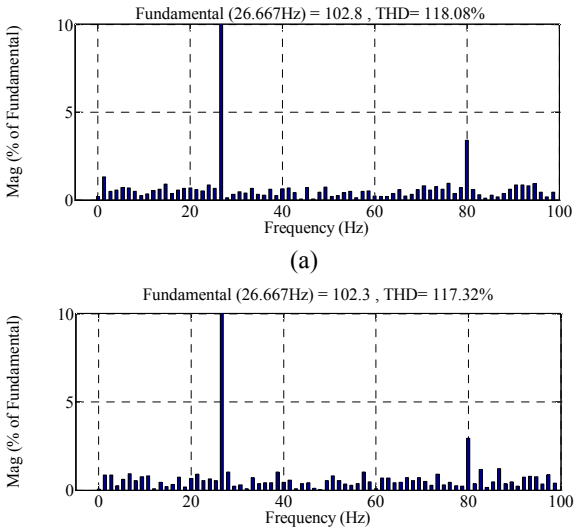

Fig. 9. Harmonic spectrum results for Phase A voltage for M1 using (a) SPWM and (b) SVPWM.

TABLE III

PHASE VOLTAGE THD COMPARISON FOR SPWM AND SVPWM

Phase		**M1**	
		S	**SV**
A	RMS	102.8 V	102.3 V
	THD	118.08%	117.32%
B	RMS	101.9 V	102.5 V
	THD	116.48%	115.50%
C	RMS	97.16 V	96.67 V
	THD	117.11%	116.86%

random spike voltage pattern.

Fig. 10 shows the simulation result of phase A current for both techniques. Similar responses are produced by both techniques either in transient or steady state. The steady-state current reaches 2 A in both cases.

IV. EXPERIMENTAL SETUP AND RESULT

The proposed SVPWM TAM is validated by the experimental setup shown in Fig. 11. The experimental setup of the drive system consists of two similar 1.5 kW Baldor induction motors, a 2.2 kW Baldor permanent magnet DC motor, a three-phase rectifier module (SEMiX341D16s), a DC link capacitor (2200 µF, 450 V DC), an insulated bipolar

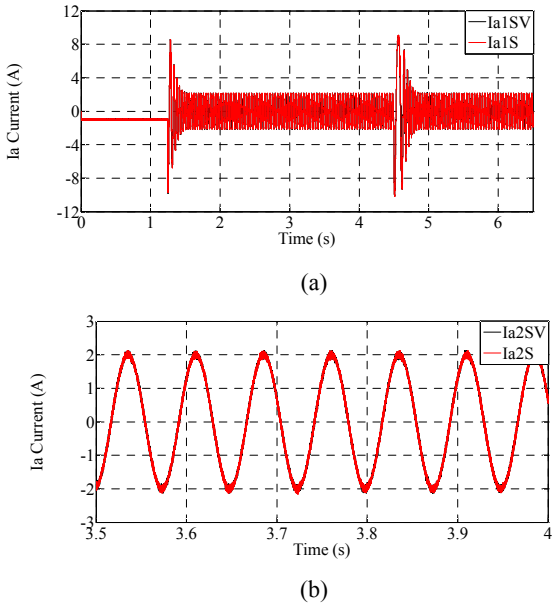

Fig. 10. Simulation results of phase A current. (a) Overall current performance of Ia for M1 and (b) zoomed extract of current Ia for M2.

transistor intelligent power module (Semikron SEMiX252GB126HDs), a current sensor circuit (LEM HY-10P) with a low-pass filter, an incremental optical encoder (E3-500-500-IE-H-T-B), and a dSPACE 1103 DSP controller. In the experiment, similar block diagrams and parameters are used with dSPACE block sets in MATLAB/Simulink. The SVPWM-generated signal is connected to the DSP1103 bit out-module from Real-Time Interface libraries. The C code is generated by Real-Time Workshop to produce switching signals. These switching signals trigger the gated drive to control FLI, which is connected to the digital input–output of the CLP1103 dSPACE controller. The voltage supply is set to its maximum capability to produce 560 V DC. The switching frequency is set to 6 kHz, and the sampling time is set to 50 µs.

A. Experimental Results

For this experiment, motor M1 is required to operate from standstill to a forward 800 rpm step speed demand and then reverse its speed operation. Motor M2 is operated at 400 rpm with constant speed. Fig. 12 shows the comparison of experiment results between SPWM and SVPWM using TAM.

The results in Fig. 12(a) show that the motor tracks the command speed with almost zero speed error during steady state with similar settling time for both forward and reverse speed operations. Motor M2 operates at a fixed speed of 400 rpm and does not affect the speed change for motor M1. The simulation produced a higher percent of overshoot, 12.25%, during forward operation compared with 8.75% of the

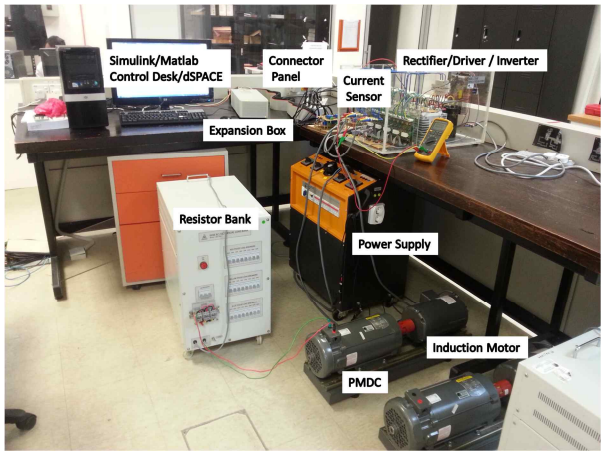

Fig. 11. Hardware experimental setup.

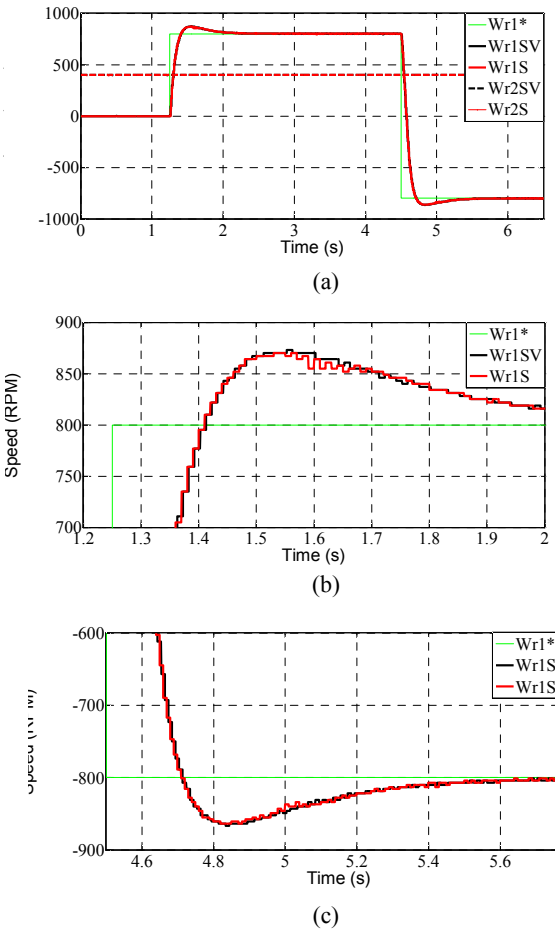

Fig. 12. Experiment results of motor speed responses. (a) Overall response of M1 and M2 motors, (b) zoomed response at forward direction for M1, and (c) zoomed response at reverse direction for M1.

experiment. A similar situation occurred during reverse operation, where the simulation and experimentation produced 12.5% and 8% overshoot, respectively, as shown in Fig. 12(c). The performance of the motor responses, such as settling time and percent overshoot obtained, are related to

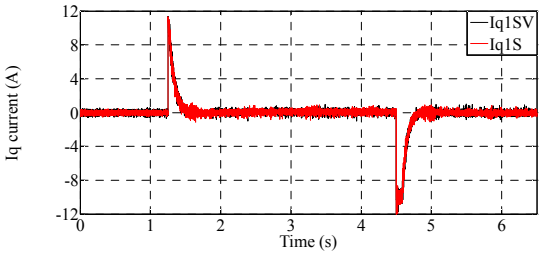

(a)

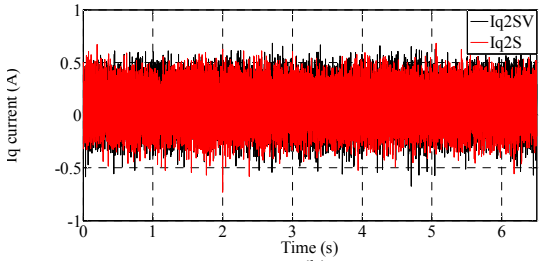

(b)

Fig. 13. Experiment results of torque current Iq in the abovementioned speed condition: (a) M1 and (b) M2.

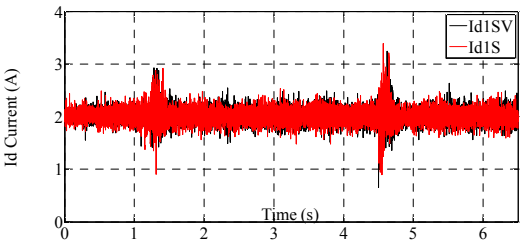

(a)

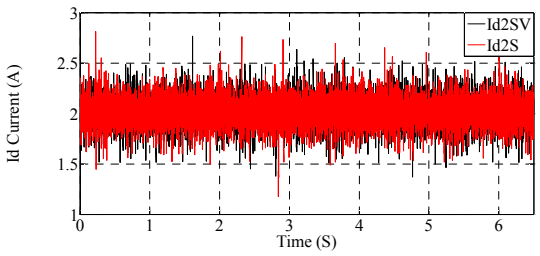

(b)

Fig. 14. Experiment results of flux component current Id in the abovementioned speed condition: (a) M1 and (b) M2.

the PI controller value.

Figs. 13(a) and 13(b) show the torque current Iq in the experimental results for motors M1 and M2. The torque current that reached a limited 10 A set at the speed controller increased tremendously during the speed step demand change. However, a larger torque ripple was recorded for the experiment result with 0.8 App compared with the 0.26 App for the simulation. The larger ripple in the experiment is due to the inconsistency of the voltage supply, switching pattern, and measurement method that normally occurs in actual experiments.

A similar effect of the torque ripple can also be observed

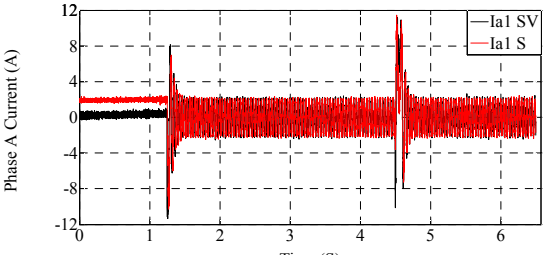

(a)

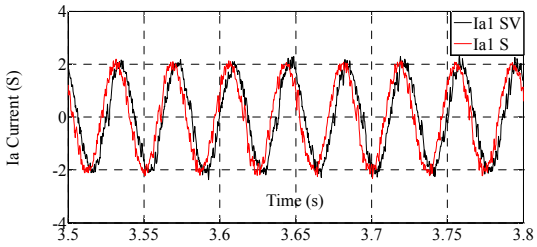

(b)

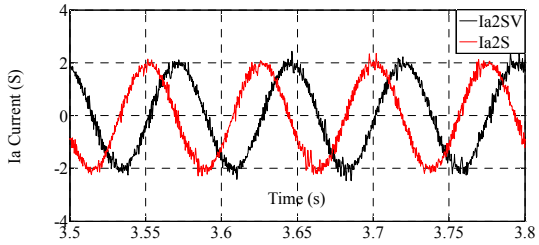

(c)

Fig. 15. Experiment results of phase A current. (a) Overall current performance of Ia for M1, (b) zoomed extract of current Ia for M1, and (c) zoomed extract of current Ia for M2.

for flux component current Id as shown in Fig. 14. The Id current relies on 2 A as the reference set value. During transition, a strong ripple effect occurs at Id1 for both methods because of coupling effect.

Fig. 15 shows the phase A current of motors M1 and M2 using SVPWM and SPWM. Figure 15(a) shows the overall current performance of motor M1 during the step speed demand change. Fig. 15(b) provides a close-up view of M1 in steady state. Fig. 15(c) provides a close-up view of the phase A current of motor M2. The sinusoidal shape of the experimental current in both techniques is similar; some phase shift is observed because of transient effect.

Fig. 16 shows the harmonic spectrum of the phase A current waveform from the experimental results obtained by SVPWM and SPWM. The fundamental current for motor M1 obtained by SVPWM is 1.99 A and that obtained by SPWM is 1.994 A.

Table IV shows the comparison of current THD between SPWM and SVPWM for M1 and M2 operation with FLI. The results show that SVWPM produced less THD than SPWM.

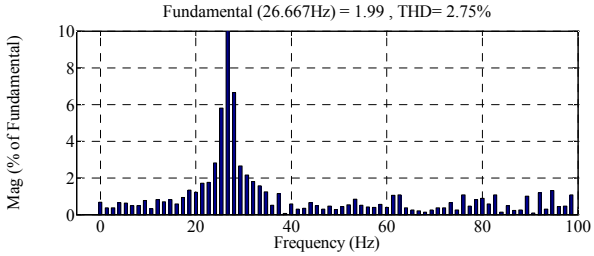

(a)

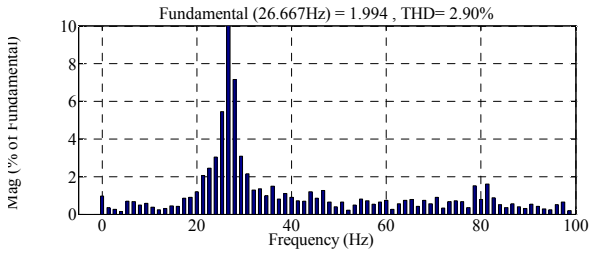

(b)

Fig. 16. Harmonic spectrum of the phase A current component: (a) M1 SVPWM and (b) M1 SPWM.

TALBE IV
COMPARISON OF THD BETWEEN SPWM AND SVPWM

Phase		M1		M2	
		S	**SV**	**S**	**SV**
A	RMS	1.994 A	1.990 A	1.945 A	1.945 A
	THD	2.90%	2.75%	2.70%	2.29%
B	RMS	1.985 A	1.989 A	1.956 A	1.946 A
	THD	2.91%	2.89%	2.85%	2.51%
C	RMS	1.898 A	1.986 A	1.950 A	1.959 A
	THD	2.44%	2.61%	2.75%	2.14%

B. Voltage Utilization Factor

This analysis is conducted when both M1 and M2 operate at 600 rpm in the forward direction. During the same-speed operation, both motors consume similar voltage. Figs. 17(a) and 17(b) show the three-phase rms voltage for M1 by SVPWM and SPWM, respectively. Fluke 435 Power Quality Analyzer is used to measure the voltage. The phase voltage measurement results indicate that both techniques produce almost similar output rms voltages with only a ±1.5 V difference, which might be due to the instantaneous switching effect. Phase C experiences high voltage of about 13 V to 16 V because of the zero voltage signal effect.

A Tektronik high-voltage differential probe and DPO 4054 Digital Phosphor Oscilloscope are utilized to measure the

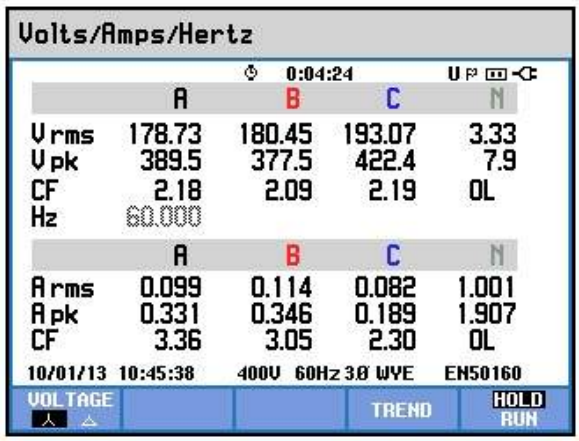

(a)

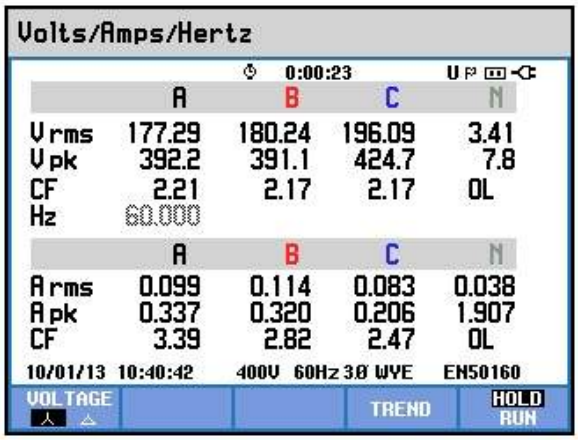

(b)

Fig. 17. Phase A voltage waveform for M1 using (a) SVPWM and (b) SPWM.

AB line voltage. The measurement results are shown in Fig. 18. The high-voltage probe employs a 500 V to 1 V voltage ratio. With this instantaneous voltage, SVPWM yields 556.50 V, and SPWM produces 551.75 V. Almost similar peak output voltages are produced, and the difference is mainly caused by switching and DC fluctuation.

According to the experimental results, the proposed carrier-based SVPWM with TAM shows a good correlation between simulation and experimentation. This technique utilizes standard three-phase modulators to successfully generate modulation signals for FLI. The dynamic behaviors of the independent speed control of the two induction motors are comparable with those of SPWM.

V. CONCLUSION

A carrier-based SVPWM technique with two-arm modulation was implemented in this study. The modulation method was used to control FLI in a two-induction drive system. The proposed method effectively controls motor speed independently. The simulation and experimental

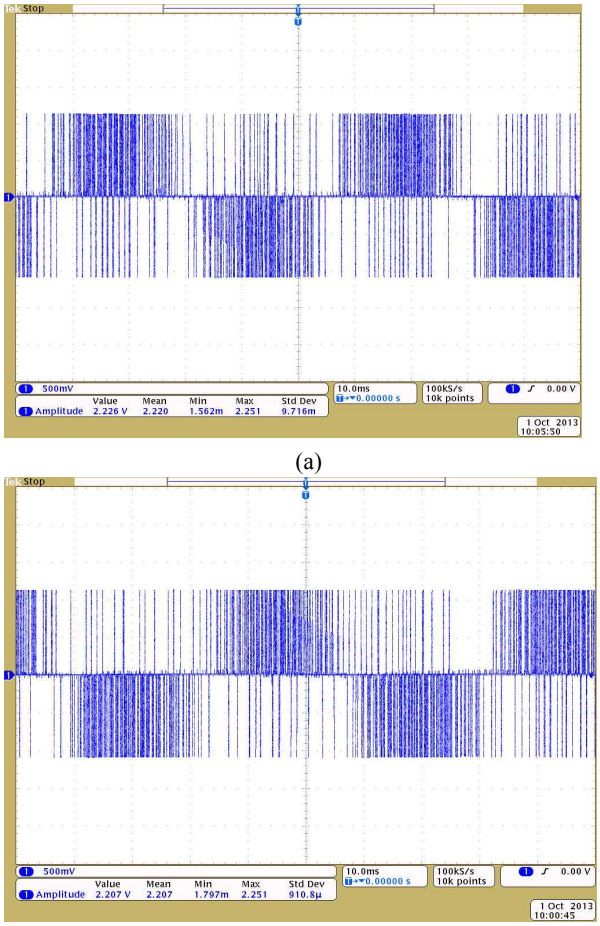

Fig. 18. Phase A voltage waveform for M1 using (a) SPWM and (b) SPWM.

results indicate that the motor performance and voltage utilization factors of the proposed technique are comparable with those of SPWM method. The speed, flux current, torque current, and voltage utilization factor performance response were analyzed. The similar voltage utilization factor in SVPWM is due to the TAM technique, which cancels out the zero-vector signals in the modulation. Both techniques have similar capabilities in following various step speed demand operations and forward/reverse operations under the speed limitation of FLI.

ACKNOWLEDGEMENTS

The authors would like to express their gratitude to the Faculty of Electrical Engineering, Universiti Teknikal Malaysia Melaka, for providing resources and support to this study.

REFERENCES

[1] D. Dujic, M. Jones, E. Levi, and S. N. Vukosavic, "A two-motor centre-driven winder drive with a reduced switch count," *IEEE Industrial Electronics Conference (IECON)* pp. 1106-1111, 2008.

[2] M. Jones, S. N. Vukosavic, D. Dujic, E. Levi, and P. Wright, "Five-leg inverter PWM technique for reduced switch count two-motor constant power applications," *IET Electric Power Applications,* Vol. 2, No. 5, pp. 275-287, Sep. 2008.

[3] C. B. Jacobina, I. S. de Freitas, E. R. C. da Silva, A. M. N. Lima, and R. L. D. A. Ribeiro, "Reduced switch count DC-link AC–AC five-leg converter," *IEEE Trans. Power Electron.,* Vol. 21, No. 5, pp. 1301-1310,Sep. 2006.

[4] L. Chee Shen, N. A. Rahim, H. Wooi Ping, and E. Levi, "Model predictive control of a two-motor drive with five-leg-inverter supply," *IEEE Trans. Ind. Electron.,* Vol. 60, No. 1, pp. 54-65, Jan. 2013.

[5] M. H. N. Talib, Z. Ibrahim, N. Abdul Rahim, and N. M. Yaakop, "Development of combined vector and Direct Torque Control methods for independent two induction motor drives," *IEEE International Power Engineering and Optimization Conference (PEOCO)* pp. 78-83, 2012.

[6] N. M. Yaakop, Z. Ibrahim, M. Sulaiman, and M. H. N. Talib, "Speed performance of SVPWM direct torque control for five leg inverter served dual three-phase induction motor," *IEEE InternationalPower Engineering and Optimization Conference (PEOCO)*, pp. 323-328, 2012.

[7] Y. Kimura, M. Hizume, and K. Matsuse, "Independent vector control of two PM motors with five-leg inverter by the expanded two-arm modulation method," *European Conference on Power Electronics and Applications*, pp. 1-7, 2005.

[8] K. Oka, Y. Nozawa, and K. Matsuse, "An improved method of voltage utility factor for PWM control of a five-leg inverter in two induction motor drives," *IEEJ Transactions on Electrical and Electronic Engineering,* Vol. 1, pp. 108-111,May 2006.

[9] Y. Ohama, K. Oka, and K. Matsuse, "Characteristic of independent two induction motor drives fed by a five-leg inverter," *International Conference on Electrical Machines and Systems (ICEMS),* , pp. 1-4, 2009.

[10] A. Hara, H. Enokijima, and K. Matsuse, "Independent vector control of two induction motors fed by a five-leg inverter with space vector modulation," *Industry Applications Society Annual Meeting (IAS)*, pp. 1-8, 2011.

[11] K. Oka and K. Matsuse, "A novel PWM technique with switching-loss reduction for independent drive of two 3-phase AC motors fed by a five-leg inverter," *IEEJ Trans. Electrical and Electronic Engineering,* Vol. 6, No. 3, pp. 260-265, May 2011.

[12] M. H. N. Talib, Z. Ibrahim, N. Abd. Rahim, and A. S. Abu Hasim, "Characteristic of Induction Motor Drives Fed by Three Leg and Five Leg Inverters," *Journal of Power Electronics,* Vol. 13, No. 5, pp. 806-813, Sep. 2013.

[13] M. Jones, D. Dujic, and E. Levi, "A performance comparison of PWM techniques for five-leg VSIs supplying two-motor drives," *IEEE Industrial Electronics Conference (IECON)*, pp. 508-513, 2008.

[14] P. Delarue, A. Bouscayrol, and E. Semail, "Generic control method of multileg voltage-source-converters for fast practical implementation," *IEEE Tran. Power Electronics,* Vol. 18, No. 2, pp. 517-526,Mar. 2003.

[15] M. Jones, D. Dujic, E. Levi, M. Bebic, and B. Jeftenic, "A two-motor centre-driven winder drive fed by a five-leg voltage source inverter," *European Conference on Power Electronics and Applications*, pp. 1-10, 2007.

[16] P. Delarue, A. Bouscayrol, and B. Francois, "Control

implementation of a five-leg voltage-source-inverter supplying two three-phase induction machines," *IEEE International Electric Machines and Drives Conference (IEMDC)*, Vol. 3, pp. 1909-1915, 2003.
[17] M. H. N. Talib, Z. Ibrahim, N. A. Rahim, and A. S. A. Hasim, "Analysis on speed characteristics of Five Leg Inverter for different carrier based PWM scheme," *IEEE International Power Engineering and Optimization Conference (PEOCO)*, pp. 96-101, 2012.
[18] H. W. van der Broeck, H. C. Skudelny, and G. V. Stanke, "Analysis and realization of a pulsewidth modulator based on voltage space vectors," *IEEE Trans. Ind. Appl.,* Vol. 24, No. 1, pp. 142-150, Jan/Feb. 1988.
[19] J. Holtz, "Pulsewidth modulation-a survey," *IEEE Trans. Ind. Electron.,* Vol. 39, No. 5, pp. 410-420, Oct. 1992.
[20] D. G. Holmes, "The significance of zero space vector placement for carrier-based PWM schemes," *IEEE Trans. Ind. Appl.,* Vol. 32, No. 5, pp. 1122-1129, Sep./Oct. 1996.
[21] Z. Keliang and W. Danwei, "Relationship between space-vector modulation and three-phase carrier-based PWM: a comprehensive analysis [three-phase inverters]," *IEEE Trans. Ind. Electron.,* Vol. 49, No. 1, pp. 186-196, Feb. 2002.
[22] E. R. C. da Silva, E. Cipriano dos Santos, and C. B. Jacobina, "Pulsewidth Modulation Strategies," *IEEE Ind. Electron. Mag.,* Vol. 5, No. 2, pp. 37-45, Jun. 2011.

Md Hairul Nizam Talib was born in Malaysia in 1976. He received his B.S. degree in electrical engineering from Universiti Teknologi Malaysia in 1999 and his M.S. degree in electrical engineering from University of Nottingham, UK, in 2005. He is working for his Ph.D. degree in Universiti Teknikal Malaysia Melaka, where he has been a lecturer since 2002. His research interests include power electronics, fuzzy logic control, and motor drives.

Zulkifilie Ibrahim was born in Malaysia in 1966. He received his B.S. degree in engineering from University of Technology, Malaysia, in 1989 and his Ph.D. degree from Liverpool John Moores University, UK, in 1999. He has been an associate professor at Universiti Teknikal Malaysia Melaka, Malaysia, since 2006. His main research interests are power electronics, fuzzy logic control, embedded system design, and electric motor drives.

Nasrudin Abd. Rahim was born in Johor, Malaysia, in 1960. He received his B.S. (with honors) and M.S. degrees from University of Strathclyde, Glasgow, U.K., and his Ph.D. degree from Heriot-Watt University, Edinburgh, U.K., in 1995. He is a professor in University of Malaya Kuala Lumpur, Malaysia, and is the Director of the University of Malaya Power Energy Dedicated Advanced Centre. He is also an adjunct professor at King Abdulaziz University, Jeddah, Saudi Arabia. Prof. Rahim is a senior member of IEEE, a fellow of the Institution of Engineering and Technology, U.K., and a fellow of the Academy of Sciences Malaysia. He is also a chartered engineer.

Ahmad Shukri Abu Hasim received his diploma, bachelor's degree, and master's degree in electrical engineering major in power from Universiti Teknologi Mara, Malaysia, in 2000, 2004, and 2008, respectively. He is a lecturer at Universiti Pertahanan Nasional Malaysia and is pursuing his Ph.D. at Universiti Teknikal Malaysia Melaka. His areas of interest are power electronic and drive systems.